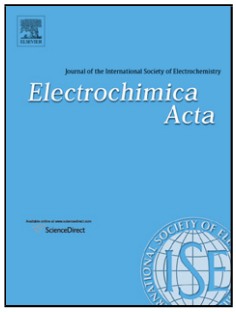

Title: Performance of Flexible and Binderless Polypyrrole/Graphene Oxide/Zinc Oxide Supercapacitor Electrode in a Symmetrical Two-Electrode Configuration

Author: W.K. Chee H.N. Lim I. Harrison K.F. Chong Z. Zainal C.H. Ng N.M. Huang

PII: S0013-4686(15)00100-0
DOI: http://dx.doi.org/doi:10.1016/j.electacta.2015.01.080
Reference: EA 24132

To appear in: *Electrochimica Acta*

Received date: 29-10-2014
Revised date: 17-1-2015
Accepted date: 18-1-2015

Please cite this article as: W.K.Chee, H.N.Lim, I.Harrison, K.F.Chong, Z.Zainal, C.H.Ng, N.M.Huang, Performance of Flexible and Binderless Polypyrrole/Graphene Oxide/Zinc Oxide Supercapacitor Electrode in a Symmetrical Two-Electrode Configuration, Electrochimica Acta http://dx.doi.org/10.1016/j.electacta.2015.01.080

Performance of Flexible and Binderless Polypyrrole/Graphene Oxide/Zinc Oxide Supercapacitor Electrode in a Symmetrical Two-Electrode Configuration

Chee W.K.[1], Lim H. N.[1,2,*], Harrison I.[3], Chong K.F.[4], Zainal Z.[1], Ng C.H.[1], Huang N.M.[5]

[1]Department of Chemistry, Faculty of Science, Universiti Putra Malaysia, 43400 UPM Serdang, Selangor, Malaysia

[2]Functional Device Laboratory, Institute of Advanced Technology, Universiti Putra Malaysia, 43400 UPM Serdang, Selangor, Malaysia

[3]Faculty of Engineering, The University of Nottingham Malaysia Campus, Jalan Broga, 43500 Semenyih, Selangor, Malaysia

[4]Faculty of Industrial Sciences & Technology, Universiti Malaysia Pahang, 26300 Gambang, Kuantan, Pahang, Malaysia.

[5]Low Dimension Materials Research Centre, Department of Physics, Faculty of Science, University of Malaya, Kuala Lumpur 50603, Malaysia

*Corresponding author: janet_limhn@yahoo.com

Graphical abstract

Abstract

A fast and facile approach based on potentiostatic electrochemical polymerization was used to prepare a polypyrrole/graphene oxide/zinc oxide (PPy/GO/ZnO) nanocomposite deposited on a flexible nickel foam. Fourier transform infrared spectroscopy and energy dispersive X-ray spectroscopy revealed the presence of zinc oxide on the PPy/GO/ZnO nanocomposite. A supercapacitor was fabricated by sandwiching a filter paper immersed in a sodium sulfate solution between two nickel foam electrodes coated with the PPy/GO/ZnO nanocomposite. The electrochemical performance of the supercapacitor was characterized using a two-

electrode configuration, and the cyclic voltammetry curve recorded at a fast scan rate of 100 mV/s was pseudo-rectangular. A specific capacitance of 94.6 F/g at a current density of 1 A/g was obtained from constant current charge/discharge measurements. The utilization of the pseudo-capacitive behavior of the polypyrrole and zinc oxide, and the electrical double layer capacitance of the graphene oxide, gave rise to a high energy and power density of 10.65 wh/kg and 258.26 w/kg at 1 A/g, respectively. The capacitance of the supercapacitor after 1000 galvanostatic charge/discharge cycles was 74% of its original value. The potential application of the as-fabricated supercapacitor in realistic energy delivery systems was demonstrated by its ability to light up a light emitting diode for about 2 minutes after being charged for approximately 30 seconds.

Keywords: Supercapacitor electrode; Zinc oxide; Graphene oxide; Polypyrrole, Binderless.

1. Introduction

The increase in carbon dioxide in the atmosphere and its detrimental effects on the climate, coupled with the environmental impact of the heavy metals used in older electronic equipment, has resulted in a growing interest in the development of low-production cost energy storage devices that use environmentally benign materials [1]. Supercapacitors have recently received a great deal of attention because of their high energy density, good cycle stability, and power handling performance [2, 3]. Generally, supercapacitors are classified into two types: pseudo-capacitors and electrical double layer capacitors (EDLC). The mechanism of a pseudo-capacitor involves faradaic charging/discharging between the electrolyte and electrode. In an EDLC, the charge is stored at the surface of the active

material by means of the absorption/desorption of ions to form electrical double layers [4, 5]. Therefore, the electrode/electrolyte interface charging mechanism has excellent stability because the reaction mainly occurs within the electrode interfaces.

The electrodes of a pseudo-capacitor are usually formed using metal oxides and conductive polymers. The multiple stable valance states of metal oxides, especially transition metal oxides, means there are a significant number of redox reactions, which results in a higher energy density compared to EDLC-based electrodes [6]. Moreover, transition metal oxides are abundant in nature and so are readily available and relatively cheap. There are, however, drawbacks to using electrodes based on metal oxides. They have a low cycling stability, which is attributed to the redox reactions not being fully reversible, along with poor electrical conductivity. Most transition metal oxides belong to a class of semiconductors that have a wide band gap energy [4], which results in low electron and hole concentrations, causing a low conductivity. Conductive polymers solve the low-conductivity problem of the electrode material while retaining the advantage of storing a charge via rapid faradic charge transfer. However, conductive polymers also have problems because they are generally brittle, with low mechanical strengths [7], and consequently have a poor charge/discharge cycling stability caused by mechanical damage to the electrode material as an effect of the continuous influx and outflow of electrolyte ions [8].

The cyclic stability and good electrical conductivity of EDLC materials such as carbon nanotubes and activated carbon (ActC) have prompted significant interest in these devices. However, the applications of these materials are limited by their capacitance values [9]. Meanwhile, graphene consisting of sp^2-hybridized carbon atoms in a two-dimensional

honeycomb structure [10] has excellent electrical and mechanical properties [11]. The zero energy band gap and electron mobility of approximately 15,000 cm^2V^{-1} produce a high conductivity. This high conductivity, coupled with a superb mechanical strength of 1.0 TPa, Young's modulus of 130 GPa, and theoretical specific surface area of 2620 m^2g^{-1}, suggest the use of graphene in future electronic devices [12].

In this study, a benign single-step electrochemical polymerization was used to synthesize a polypyrrole/graphene oxide/zinc oxide nanocomposite. The properties of this nanocomposite should combine the benefits of the pseudo-capacitance arising from the inclusion of ZnO and the EDLC formed at the surface of the graphene. To characterize the electrochemical performance of the nanocomposite, a simple two-electrode electrochemical cell was constructed using the nanocomposite as the electrodes. A nickel foam was used as a deposition substrate to provide mechanical strength and act as a current collector. The electrodes were separated by a dielectric filter membrane saturated with a sodium sulfate solution, which acted as both a porous ion separator and electrolyte reservoir.

2. Materials and methods

2.1 Materials

Graphite powder was obtained from Ashbury Graphite Mills Inc (code no. 3061), United States. Sulfuric acid (H_2SO_4, 95%–98%), phosphoric acid (H_3PO_4, 85%), charcoal activated powder (ChemPur), potassium permanganate ($KMnO_4$, 99.9%), hydrogen peroxide (H_2O_2, 30%), and hydrochloric acid (HCl, 37%) were purchased from Systerm, Malaysia. Sodium p-toluenesulfonate (NapTS), zinc sulfate heptahydrate ($ZnSO_4.7H_2O$), and sodium sulfate (Na_2SO_4) were provided by Merck, Malaysia. Pyrrole (99%) was purchased from Acros

Organic, New Jersey, USA stored at 0 °C, and distilled before use. Nickel foam was purchased from Goodfellow Cambridge Ltd, UK. Nylon membrane filter was obtained from Membrane Solutions, LLC, USA.

2.2 Synthesis of graphene oxide (GO)

GO was synthesized via a modified Hummer's method [13], where 3 g of graphite flakes was oxidized by the addition of an acid mixture of H_2SO_4:H_3PO_4 (9:1) and 18 g of $KMnO_4$. The mixture was stirred continuously for about 5 min to complete the oxidation process. H_2O_2 solution was added to stop the oxidation process, at which time the color of the solution changed from dark brown to milky yellow. The mixture obtained was then washed with a 1 M HCl solution, using a centrifuge, followed by repeated washing with de-ionized water until a constant pH of 4–5 was obtained. After washing, the graphite oxide experienced exfoliation, forming a GO gel. The concentration of GO was 5.50 mg/ml.

2.3 Preparation of PPy/GO/ZnO on nickel foam

A PPy/GO/ZnO nanocomposite was electro-potentiostatically deposited on the nickel foam from an aqueous solution. The aqueous solution contained 0.1 $moll^{-1}$ of PPy, 0.1 $moll^{-1}$ of NapTS as a supporting electrolyte, 1 mg/ml of GO, and 0.1 $moll^{-1}$ of $ZnSO_4$. A potentiostat–galvanostat (AUTOLAB Metrohm PGSTAT204) was used for the electrodeposition, in which the nickel foam was the working electrode, a platinum rod was used as the counter electrode, and a saturated calomel electrode (SCE) was the reference electrode. The electrochemical deposition was carried out at a constant potential of +0.8 V (E versus SCE) at ambient temperature for 15 min. PPy and PPy/GO were also prepared for comparison with PPy/GO/ZnO. An ActC electrode, formed by soaking the nickel foam in a slurry containing

ActC powder and de-ionized water for 30 min and left to dry under ambient conditions, was prepared as a positive control.

2.4 Material characterizations

The surface morphologies of the nanocomposites were analyzed using a field emission scanning electron microscope (FEI Quanta SEM Model 400F) equipped with an energy dispersive X-ray (EDX) feature. The Fourier transform infrared spectroscopy (FT-IR) spectra of the samples were recorded using the attenuated total reflectance (ATR) on a Fourier transform infrared spectrophotometer (Perkin Elmer 1650). The spectra were recorded over the range of 280–4000 cm^{-1}.

2.5 Preparation of supercapacitor

The as-prepared nanocomposite deposited on the nickel foam was used as the electrodes in a supercapacitor. Two identical electrodes were separated by a piece of filter paper soaked overnight in 1 $moll^{-1}$ of a Na_2SO_4 solution prior to use. The electrode configuration was placed securely into a Swagelok cell and subjected to electrochemical characterizations using a two-electrode configuration.

2.6 Electrochemical characterization

The electrochemical properties of the prepared nanocomposites were characterized using the same potentiostat–galvanostat apparatus used in the deposition of the samples. Cyclic voltammetry (CV), electrochemical impedance spectroscopy (EIS), and galvanostatic

charge/discharge measurements were carried out using a two-electrode configuration. CV was perform at a working potential of -0.2 V to +0.7 V with scan rates between 2 mV/s and 100 mV/s. EIS was performed from 5 mHz to 100 kHz, with an AC amplitude of 5 mV. Galvanostatic charge/discharge cycling of the two-electrode system was carried out from 0 V to 0.9 V, and the specific capacitance (C_m) was calculated from the discharge curve using Eq. 1 [14, 15], where *I* is the applied current, and *dV/dt* is the slope of the discharge curve (V/s).

$$\text{Specific Capacitance (F/g)} = \frac{I}{-dV/dt} \quad (1)$$

The energy density (E) and power density (P) of the electrochemical cell were calculated from the charge/discharge profiles using Eq. 2 [16, 17]:

$$E_{cell}\,(\text{Wh/kg}) = \tfrac{1}{2}\, C_{C/DC}\, V^2$$

$$P_{cell}\,(\text{W/kg}) = E_{cell}/\,\Delta t \quad (2)$$

Where $C_{C/DC}$ is the specific capacitance of a cell calculated from charge/discharge measurements, V is the potential window, and Δt is the discharge time.

3. Results and Discussion

During the electro-deposition, the nanocomposite was deposited uniformly and completely on the surface of the nickel foam facing the counter-electrode (front-facing surface). In contrast, the surface of the nickel foam facing away from the counter-electrode (back-facing surface) was not entirely covered with the nanocomposite because traces of nickel were still visible to the unaided eye. The EDX spectra clearly show that the intensity of the nickel foam (circled in blue for clarity) on the front-facing surface is much lower than that of the back-facing surface, for both PPy/GO (Figure 1a) and PPy/GO/ZnO (Figure 1b). Unlike the deposition of

PPy on nickel foam (Figure 2a), the addition of GO generated a fibrous morphology, and there is no clear distinction between the PPy and GO (Figure 2b), indicating that the components blended into each other. Similarly, PPy/GO/ZnO had a fibrous structure (Figure 2c), but the introduction of ZnO led to a coarser fibrous material. The presence of Zn in these courser fibers is substantiated by the elemental map shown in Figure 2d. The difference in morphology between the GO-containing samples and those containing only PPy can be explained by the formation mechanism of PPy during the electrostatic deposition. As reported in detail in our earlier work [18], the chain growth of PPy is continued by the addition of newly formed radical cations of pyrrole monomers to the existing oligomeric chains. This explains the continuous growth and thick layers of PPy within the micropores of the nickel foam. Upon the introduction of GO, negatively charged GO would be attracted to the pyrrole radical cations during the electro-deposition. The GO flakes compete with the existing PPy oligomeric chains, which results in portions of the pyrrole monomers being deposited on the surface of the GO. Eventually, a new layer of PPy would form when the existing GO surface was fully occupied by PPy, and this was a continuous process. The continuous growth of PPy on the existing chains was disrupted and no longer occurred predominantly within the pores of the nickel foam. Therefore, the layer-by-layer deposition of PPy and GO were well-arranged across the surface of the nickel foam, resulting in the fibrous structure of the PPy/GO and PPy/GO/ZnO.

Figure 3 highlights the changes to the FT-IR spectrum of the nickel foam after the deposition of PPy/GO/ZnO. The characteristic peak of the octahedral-metal stretching (Ni ↔ O) was assigned to 397 cm^{-1} [19] for the blank nickel foam. However, this characteristic peak of nickel was undetectable after the deposition of PPy/GO/ZnO, suggesting a uniform deposition of the nanocomposite on the framework of the nickel foam, which complemented

the results shown in the FESEM images. The nanocomposite-coated nickel foam exhibited the characteristic peaks of pure PPy at 1494 cm^{-1} (aromatic stretching of pyrrole ring)[20], and 1119 cm^{-1} (C-N stretching)[21]. In addition, the weak ZnO absorption band was detected at 427 cm^{-1} [22-24].

An ideal capacitor will exhibit a perfect square when subjected to CV measurements, independent of the scan rate. A series resistance and diffusion of the electrolyte result in a trapezoidal shape, which closes as the scan rate increases. In real capacitors, the breakdown of the electrolyte and redox reactions at the electrodes result in an increase in the current at the edges of the scan and peaks in both the charging and discharging parts of the scan. The measured CV of the present PPy/GO/ZnO-based supercapacitor did not show any peaks that could be associated with the ZnO redox reactions.

The manufactured PPy/GO/ZnO-based supercapacitor had an open pseudo-rectangular shaped CV at various scan rates without any observable redox peaks (Figure 4a). This result was similar to the results of previously published work [18, 25-29]. Li et al. used TEM to show that ZnO nano-crystals were uniformly dispersed between GO sheets, which effectively prevented the agglomeration and restacking of the GO sheets, therefore resulting an EDLC characteristic for the overall performance [25]. As expected, the specific capacitance calculated from CV profiles (see supplementary equation S1) increased as the scan rate decreased because, at slow scan rates, there was more time for the electrolyte ions to diffuse to the electrode materials (Table 1). Furthermore, PPy/GO/ZnO had the largest enclosed area in the CV scan when measured at 2 mv/s compared to either PPy/GO or PPy, indicating an improvement in the capacitance performance (Figure 4b).

The charging/discharging performance of the PPy/GO/ZnO device was better than those of PPy/GO and PPy (Figure 5a). The PPy/GO/ZnO-based supercapacitor displayed typical galvanostatic charge/discharge curves at various current densities of 1, 2, and 5 A/g (Figure 5b), which implied exceptional charge/discharge reversibility [27, 29, 30]. The specific capacitances of the PPy/GO/ZnO, PPy/GO, and PPy were 94.6 F/g, 66.7 F/g, and 37.5 F/g, respectively. The specific capacitances of all of the samples were heavily influenced by the current density. As shown in Figure 5c, the specific capacitance decreases with increasing current density as a result of an inadequate response time for the electrolyte ions to reach the surface of the electrode at a high current rate [31]. To visualize the electrochemical potential of the electrode material, the electrochemical cells connected in series were able to light up an LED circuit, which strengthens the concept of using the PPy/GO/ZnO nanocomposite in energy delivery systems.

The specific energy density (E) is defined as the amount of energy stored per unit weight in a particular device, while the specific power density (P) is directly related to the rate at which energy can be transferred from the device. Both are commonly used as figures of merit to characterize and compare the electrochemical performances of different devices [32, 33]. The non-linear internal resistance of the storage device means there is no simple relationship between the energy density and power density. Therefore, to allow comparisons, a Ragone plot is often used, and Figure 6 presents the plots for PPy, PPy/GO, and PPy/GO/ZnO. Additionally, the data obtained for ActC are compared in supplementary Figure S1. The PPy/GO/ZnO supercapacitor had a specific energy density and specific power density of 3.85 wh/kg and 1479.29 W/kg, respectively, at a high current density of 5 A/g. At 1 A/g, PPy/GO/ZnO had an energy density and a power density of 10.65 wh/kg and 258.26 W/kg, respectively. The high specific energy density achieved at a low current rate can be attributed

to the ability of the electrolyte ions to diffuse throughout the electrode material. In contrast, at high current rates, there was insufficient time for ion diffusion, especially inside the smallest pores of the electrode materials [34], resulting in a lower specific power density. The PPy (4.22 W/kg, 257.91 Wh/kg) and PPy/GO (7.53 W/kg and 254.70 Wh/kg) samples both possessed significantly lower power density and energy density values than those of PPy/GO/ZnO at 1 A/g. This indicates that the presence of ZnO effectively enhanced the electrochemical performance by acting as a pseudo-capacitor active material and semiconductor filler to provide a smooth electrical connectivity within the electrode, as evidenced by the lower ESR and R_{ct} found using electro-impedance spectroscopy. An attempt was made to compare the performance of the fabricated PPy/GO/ZnO supercapacitor to that of a supercapacitor made using Ni foam coated with ActC powder. However, it was not possible to derive the capacitance from the charge-discharge measurements for the AC sample because of the large series resistance (large IR drop). In order to facilitate a comparison, the specific energy and specific power densities were calculated based on the capacitance derived from CV measurements (see supplementary equation S2). The fibrous structure of GO resulted in a significantly higher specific surface area, which efficiently facilitated the motions of electrolyte ions, unlike those of ActC, and led to larger figures of merit. In addition, the random pore size distribution of the ActC on the nickel foam might have caused an obstruction in the facilitation of electrolyte ions within the electrode materials [32]. Micropores with diameters smaller than 1 nm directly hinder the diffusion of electrolytes ions, leading to a lower capacitance performance [35] The Ragone profile reflected the drawback of using ActC as an active material for a supercapacitor (see supplementary Figure S1). The incorporation of ZnO into the PPy/GO improved the energy density of the system, probably because of the addition of a pseudo-capacitance [25], whereas the enhancement in the power density indicated the successive utilization of graphene oxide

to provide good electronic conductivity and the fast transfer of electrons throughout the electrodes [36]. The time constants of redox reactions often limit the power performance. The samples presented here were no different. At higher power densities, the available energy from the PPy/GO/ZnO device dropped below that of the GO/PPy device.

The impedance spectra measured for the PPy, PPy/GO, and PPy/GO/ZnO are shown as Nyquist plots in Figure 7. The high-frequency arc in pseudo-capacitors is caused by a resistive term (R_{ct}) attributed to the charge transfer limiting process at the interface of the electrode material and electrolyte [27]. Its value can be obtained from the diameter of the arc [18, 26]. All capacitors also have an equivalent series resistance (ESR), which is caused by the resistance of the solution, as well as the internal resistance of the electrode. A value can be obtained from the high-frequency impedance limit. In terms of the Nyquist plot, this corresponds to the first intercept on the X axis (real part of the impedance). In Figure 7, the low-frequency arc in the Nyquist plot associated with the PPy device exhibits a larger radius, indicating a higher charge transfer resistance than the other samples. On the other hand, the PPy/GO/ZnO device has the smallest diameter in the Nyquist plot, signifying a lower resistance and faster diffusion of ions within the electrode materials [37]. The ESR and R_{ct} values of the PPy/GO composite (ESR = 0.96 Ω, R_{ct} = 1.5021 Ω) were lower than those of PPy (ESR = 1.04 Ω, R_{ct} = 2.97 Ω). The introduction of GO provided a conductive framework for the nucleation and growth of PPy to take place, as well as a shortened diffusion path for electrolyte ions [38]. The ESR of PPy/GO/ZnO (ESR = 0.86 Ω, R_{ct} = 1.10 Ω) was lower than those of both PPy and PPy/GO, most probably because of the unique performance of the ZnO nanoparticles, which facilitated the charge transfer performance of the electrode, as depicted by the schematic in Figure 8 [29, 39].

The cycling stability and capacitive retention of supercapacitors are critical performance figures for practical energy storage applications. For PPy/GO/ZnO, the specific capacitance increased steadily up to 100 cycles as a result of the gradual infusion of electrolyte ions within the matrix of the PPy/GO/ZnO nanocomposite (Figure 9). The specific capacitance decreased after this, but retained 73.6% of its original value after 1000 continuous charge/discharge cycles at a current density of 1 A/g. Previous studies using graphene/ZnO or PPy/graphene as an electrode material recorded similar stabilities, but only over 200–400 cycles [11, 27, 40]. The reduction in the specific capacitance could have resulted from a degradation of the polymer chains and a deterioration of the active materials after excessive swelling and shrinking of the polymer during the charge/discharge test [8, 11, 12, 14]. Nevertheless, the PPy/GO/ZnO nanocomposite was still able to retain a considerable amount of specific capacitance, indicating that only a minor degradation occurred during the charge/discharge process.

4.0 Conclusion

We successfully fabricated a PPy/GO/ZnO-based supercapacitor using a fast and facile one-step electrochemical deposition under ambient conditions. The PPy/GO/ZnO nanocomposite exhibited an excellent capacitive performance of 94.6 F/g at 1 A/g. The CV curve displayed a typical pseudo-rectangular shape, which implied a rapid charging/discharging behavior. Furthermore, the PPy/GO/ZnO device outperformed PPy/GO and PPy devices by achieving an energy density of 10.65 Wh/kg and a power density of 258.26 W/kg at 1 A/g. After charging/discharging for 1000 cycles, 74% of the original capacitance was retained, which showed promising electrochemical stability attributed to the ZnO nanocrystals, which hindered the structural degradation of the polymer. The prepared electrochemical cell was

able to light up an LED circuit after being charged, demonstrating the use of this technology in real applications. These encouraging results may hold the key to the sustainable and improved fabrication of high-performance energy delivery system for electronic applications.

Acknowledgement

This research work was supported by the Prototype Research Grant Scheme (PRGS/1/2013/TK02/UPM/02/1) and a High Impact Research Grant (UM.C/625/1/HIR/MOHE/05) from the Ministry of Higher Education.

References

[1] Y. Wang, Z. Shi, Y. Huang, Y. Ma, C. Wang, M. Chen, Y. Chen, Supercapacitor Devices Based on Graphene Materials, The Journal of Physical Chemistry C, 113 (2009) 13103-13107.
[2] Z. Li, J. Wang, S. Liu, X. Liu, S. Yang, Synthesis of hydrothermally reduced graphene/MnO_2 composites and their electrochemical properties as supercapacitors, Journal of Power Sources, 196 (2011) 8160-8165.
[3] Q. Tang, L. Wang, X. Qin, Study on the Capacitance Performance of Graphene, Integrated Ferroelectrics, 136 (2012) 127-131.
[4] J. Jiang, Y. Li, J. Liu, X. Huang, C. Yuan, X.W. Lou, Recent Advances in Metal Oxide-based Electrode Architecture Design for Electrochemical Energy Storage, Advanced Materials, 24 (2012) 5166-5180.
[5] Y. Liu, D. He, H. Wu, J. Duan, Graphene and Nanostructured Mn_3O_4 Composites for Supercapacitors, Integrated Ferroelectrics, 144 (2013) 118-126.
[6] X. Wang, J. Liu, Y. Wang, C. Zhao, W. Zheng, Ni(OH)2 nanoflakes electrodeposited on Ni foam-supported vertically oriented graphene nanosheets for application in asymmetric supercapacitors, Materials Research Bulletin, 52 (2014) 89-95.
[7] J. Zhang, X.S. Zhao, Conducting Polymers Directly Coated on Reduced Graphene Oxide Sheets as High-Performance Supercapacitor Electrodes, The Journal of Physical Chemistry C, 116 (2012) 5420-5426.
[8] Y.S. Lim, Y.P. Tan, H.N. Lim, N.M. Huang, W.T. Tan, M.A. Yarmo, C.-Y. Yin, Potentiostatically deposited polypyrrole/graphene decorated nano-manganese oxide ternary film for supercapacitors, Ceramics International, 40 (2014) 3855-3864.
[9] H. Gómez, M.K. Ram, F. Alvi, P. Villalba, E. Stefanakos, A. Kumar, Graphene-conducting polymer nanocomposite as novel electrode for supercapacitors, Journal of Power Sources, 196 (2011) 4102-4108.
[10] J. Basu, J.K. Basu, T.K. Bhattacharyya, The evolution of graphene-based electronic devices, International Journal of Smart and Nano Materials, 1 (2010) 201-223.
[11] C. Zhu, J. Zhai, D. Wen, S. Dong, Graphene oxide/polypyrrole nanocomposites: one-step electrochemical doping, coating and synergistic effect for energy storage, Journal of Materials Chemistry, 22 (2012) 6300-6306.
[12] Z.-S. Wu, G. Zhou, L.-C. Yin, W. Ren, F. Li, H.-M. Cheng, Graphene/metal oxide composite electrode materials for energy storage, Nano Energy, 1 (2012) 107-131.
[13] Huang N.M., Lim H.N., Chia C.H., Yarmo M.A., M. M.R., Simple room-temperature preparation of high-yield large-area graphene oxide, International Journal of Nanomedicine, 2011:6 (2011) 3443 - 3448.

[14] D. Ghosh, S. Giri, S. Sahoo, C.K. Das, In Situ Synthesis of Graphene/Amine-Modified Graphene, Polypyrrole Composites in Presence of $SrTiO_3$ for Supercapacitor Applications, Polymer-Plastics Technology and Engineering, 52 (2013) 213-220.
[15] C.X. Guo, C.M. Li, A self-assembled hierarchical nanostructure comprising carbon spheres and graphene nanosheets for enhanced supercapacitor performance, Energy & Environmental Science, 4 (2011) 4504-4507.
[16] Z.P. Zhou, X.F. Wu, High-performance porous electrodes for pseudosupercapacitors based on graphene-beaded carbon nanofibers surface-coated with nanostructured conducting polymers, Journal of Power Sources, 262 (2014) 44-49.
[17] Y.J. Kang, S.-J. Chun, S.-S. Lee, B.-Y. Kim, J.H. Kim, H. Chung, S.-Y. Lee, W. Kim, All-Solid-State Flexible Supercapacitors Fabricated with Bacterial Nanocellulose Papers, Carbon Nanotubes, and Triblock-Copolymer Ion Gels, ACS Nano, 6 (2012) 6400-6406.
[18] Y.S. Lim, Y.P. Tan, H.N. Lim, N.M. Huang, W.T. Tan, Preparation and characterization of polypyrrole/graphene nanocomposite films and their electrochemical performance, Journal of Polymer Research, 20 (2013) 1-10.
[19] S. Maensiri, C. Masingboon, B. Boonchom, S. Seraphin, A simple route to synthesize nickel ferrite ($NiFe_2O_4$) nanoparticles using egg white, Scripta Materialia, 56 (2007) 797-800.
[20] S. Jamadade, S.V. Jadhav, V. Puri, Electromagnetic reflection, shielding and conductivity of polypyrrole thin film electropolymerized in P-Tulensulfonic acid, Journal of Non-Crystalline Solids, 357 (2011) 1177-1181.
[21] Y. Han, L. Hao, X. Zhang, Preparation and electrochemical performances of graphite oxide/polypyrrole composites, Synthetic Metals, 160 (2010) 2336-2340.
[22] A. Becheri, M. Dürr, P. Lo Nostro, P. Baglioni, Synthesis and characterization of zinc oxide nanoparticles: application to textiles as UV-absorbers, J Nanopart Res, 10 (2008) 679-689.
[23] S. Maensiri, P. Laokul, V. Promarak, Synthesis and optical properties of nanocrystalline ZnO powders by a simple method using zinc acetate dihydrate and poly(vinyl pyrrolidone), Journal of Crystal Growth, 289 (2006) 102-106.
[24] R.F. Silva, M.E.D. Zaniquelli, Morphology of nanometric size particulate aluminium-doped zinc oxide films, Colloids and Surfaces A: Physicochemical and Engineering Aspects, 198–200 (2002) 551-558.
[25] Z. Li, Z. Zhou, G. Yun, K. Shi, X. Lv, B. Yang, High-performance solid-state supercapacitors based on graphene-ZnO hybrid nanocomposites, Nanoscale Research Letters, 8 (2013) 473-482.
[26] D.P. Dubal, S.H. Lee, J.G. Kim, W.B. Kim, C.D. Lokhande, Porous polypyrrole clusters prepared by electropolymerization for a high performance supercapacitor, Journal of Materials Chemistry, 22 (2012) 3044-3052.
[27] J. Wang, Z. Gao, Z. Li, B. Wang, Y. Yan, Q. Liu, T. Mann, M. Zhang, Z. Jiang, Green synthesis of graphene nanosheets/ZnO composites and electrochemical properties, Journal of Solid State Chemistry, 184 (2011) 1421-1427.
[28] Y.-L. Chen, Z.-A. Hu, Y.-Q. Chang, H.-W. Wang, Z.-Y. Zhang, Y.-Y. Yang, H.-Y. Wu, Zinc Oxide/Reduced Graphene Oxide Composites and Electrochemical Capacitance Enhanced by Homogeneous Incorporation of Reduced Graphene Oxide Sheets in Zinc Oxide Matrix, The Journal of Physical Chemistry C, 115 (2011) 2563-2571.
[29] T. Lu, Y. Zhang, H. Li, L. Pan, Y. Li, Z. Sun, Electrochemical behaviors of graphene–ZnO and graphene–SnO_2 composite films for supercapacitors, Electrochimica Acta, 55 (2010) 4170-4173.
[30] J. Yan, Z. Fan, T. Wei, W. Qian, M. Zhang, F. Wei, Fast and reversible surface redox reaction of graphene–MnO_2 composites as supercapacitor electrodes, Carbon, 48 (2010) 3825-3833.
[31] L.L. Zhang, S. Zhao, X.N. Tian, X.S. Zhao, Layered Graphene Oxide Nanostructures with Sandwiched Conducting Polymers as Supercapacitor Electrodes, Langmuir, 26 (2010) 17624-17628.
[32] Z. Fan, J. Yan, T. Wei, L. Zhi, G. Ning, T. Li, F. Wei, Asymmetric Supercapacitors Based on Graphene/MnO_2 and Activated Carbon Nanofiber Electrodes with High Power and Energy Density, Advanced Functional Materials, 21 (2011) 2366-2375.

[33] M. Winter, R.J. Brodd, What are batteries, fuel cells, and supercapacitors?, Chemical reviews, 104 (2004) 4245-4270.
[34] D.P. Dubal, R. Holze, All-solid-state flexible thin film supercapacitor based on Mn_3O_4 stacked nanosheets with gel electrolyte, Energy, 51 (2013) 407-412.
[35] M. Liang, B. Luo, L. Zhi, Application of graphene and graphene‐based materials in clean energy‐related devices, International Journal of Energy Research, 33 (2009) 1161-1170.
[36] C. Xu, J.-H. Lee, J.-C. Lee, B.-S. Kim, S.W. Hwang, D. Whang, Electrochemical growth of vertically aligned ZnO nanorod arrays on oxidized bi-layer graphene electrode, Cryst Eng Comm, 13 (2011) 6036-6039.
[37] D. Zhang, H. Yan, Y. Lu, K. Qiu, C. Wang, C. Tang, Y. Zhang, C. Cheng, Y. Luo, Hierarchical mesoporous nickel cobaltite nanoneedle/carbon cloth arrays as superior flexible electrodes for supercapacitors, Nanoscale Res Lett, 9 (2014) 139.
[38] M.D. Stoller, S. Park, Y. Zhu, J. An, R.S. Ruoff, Graphene-Based Ultracapacitors, Nano Letters, 8 (2008) 3498-3502.
[39] Y. Zhang, H. Li, L. Pan, T. Lu, Z. Sun, Capacitive behavior of graphene–ZnO composite film for supercapacitors, Journal of Electroanalytical Chemistry, 634 (2009) 68-71.
[40] X. Wang, C. Yang, P. Liu, Facile decoration of polypyrrole nanoparticles onto graphene nanosheets for supercapacitors, Synthetic Metals, 162 (2012) 2349-2354.

Figure 1. EDX spectrum of PPy/GO (a) and EDX spectrum of PPy/GO/ZnO (b), along with the images of deposited surface (inset).

Figure 2. FESEM images of PPy (a), PPy/GO (b), PPy/GO/ZnO (c), and elemental mapping derived from EDX measurements of PPy/GO/ZnO (d).

Figure 3. FT-IR spectra of blank nickel and PPy/GO/ZnO deposited on nickel foam.

Figure 4. (a) CV profiles of PPy/GO/ZnO at various scan rates, with no observable redox peaks detected. (b) Comparison of CV profiles of PPy/GO/ZnO, PPy/GO, and PPy at a scan rate of 2 mV/s, which shows the superior performance of the PPy/GO/ZnO sample.

Figure 5. (a) Galvanostatic charge/discharge curves of PPy, PPy/GO, and PPy/GO/ZnO at current density of 1A/g, with longest discharge time recorded for PPy/GO/ZnO. (b) Charge/discharge curves of PPy/GO/ZnO at various current densities. (c) Decrease trends of specific capacitances as a function of increasing current densities.

Figure 6. Ragone plots of PPy, PPy/GO, and PPy/GO/ZnO. PPy/GO/ZnO outperforms both the PPy and PPy/GO samples by recording a significantly higher energy density and power density profile.

Figure 7. Nyquist plots of PPy, PPy/GO, and PPy/GO/ZnO.

Figure 8. Schematic diagram of charging/discharging mechanism of PPy/GO/ZnO nanocomposite.

Figure 9. Cyclic performance of PPy/GO/ZnO supercapacitor.

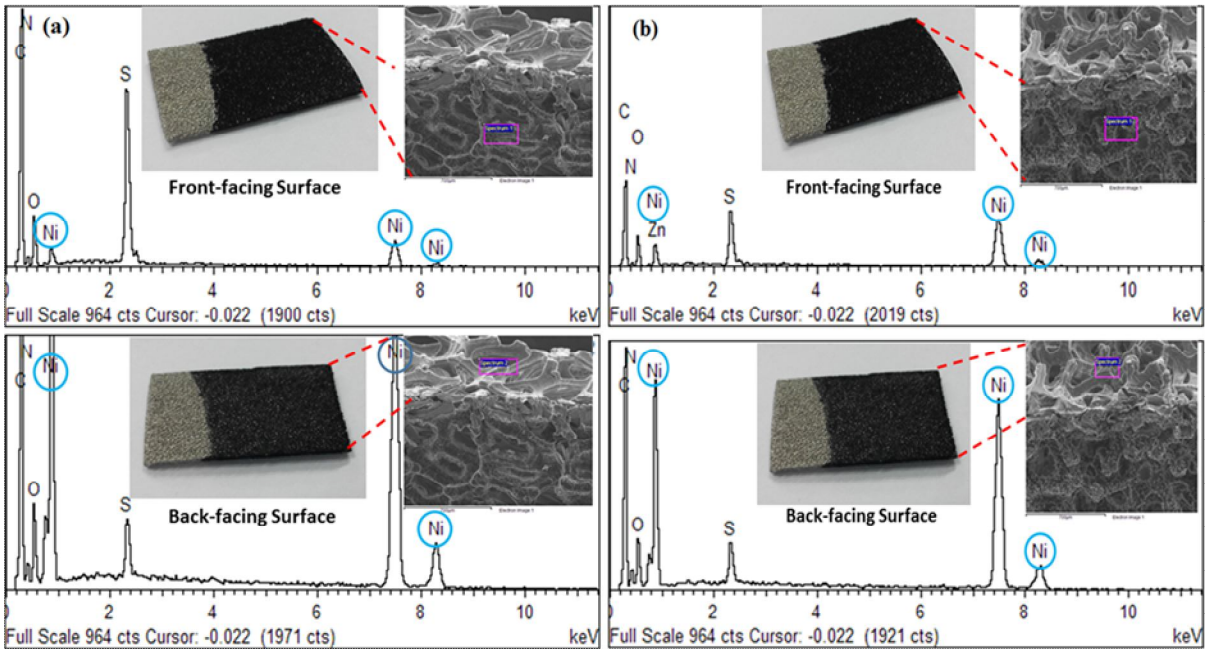

Figure 1

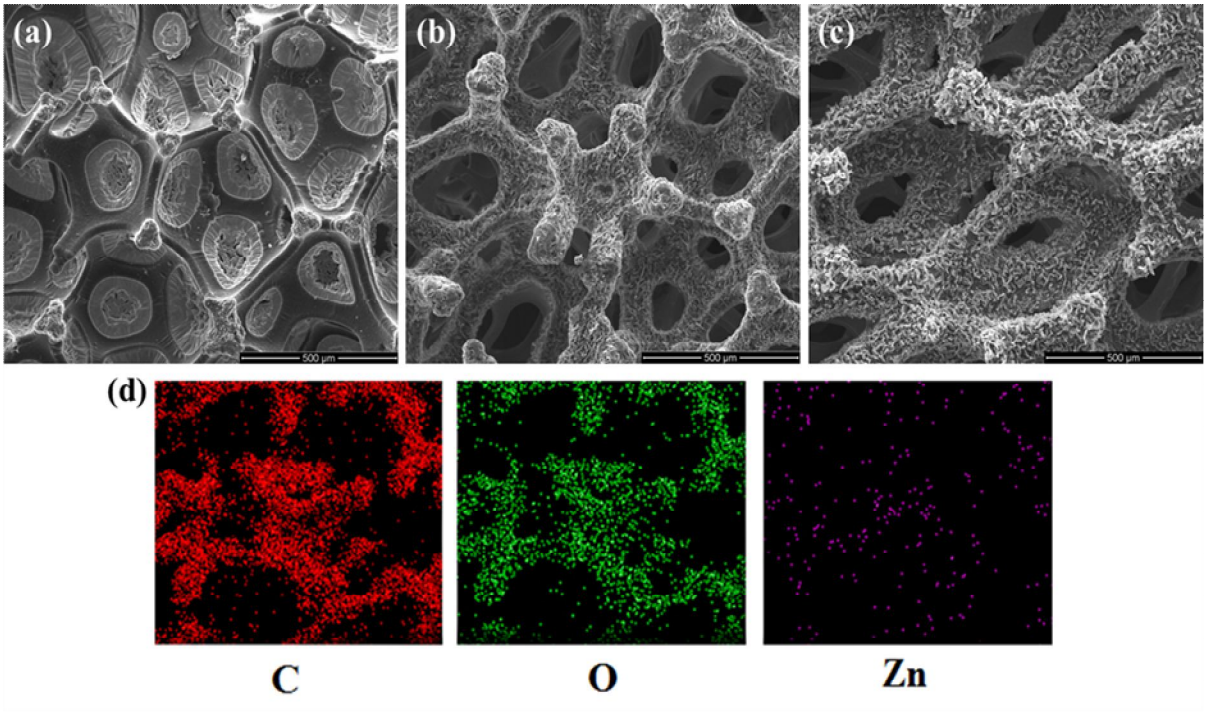

Figure 2

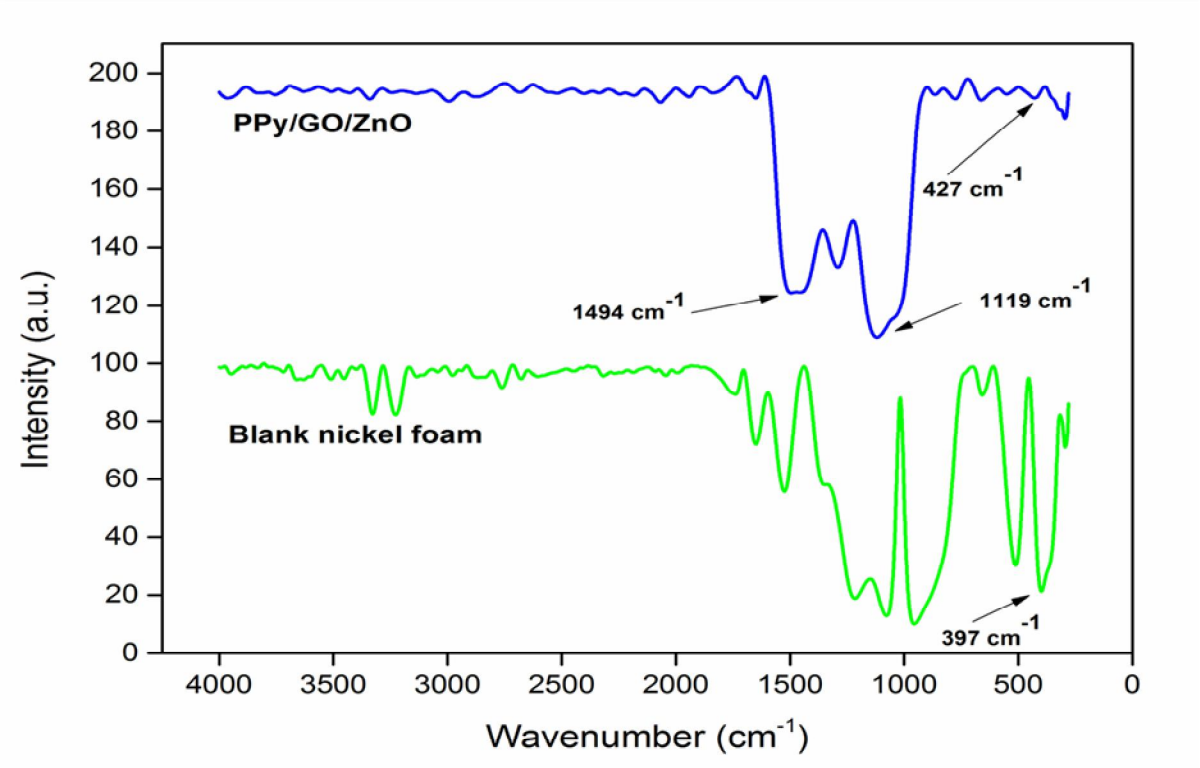

Figure 3

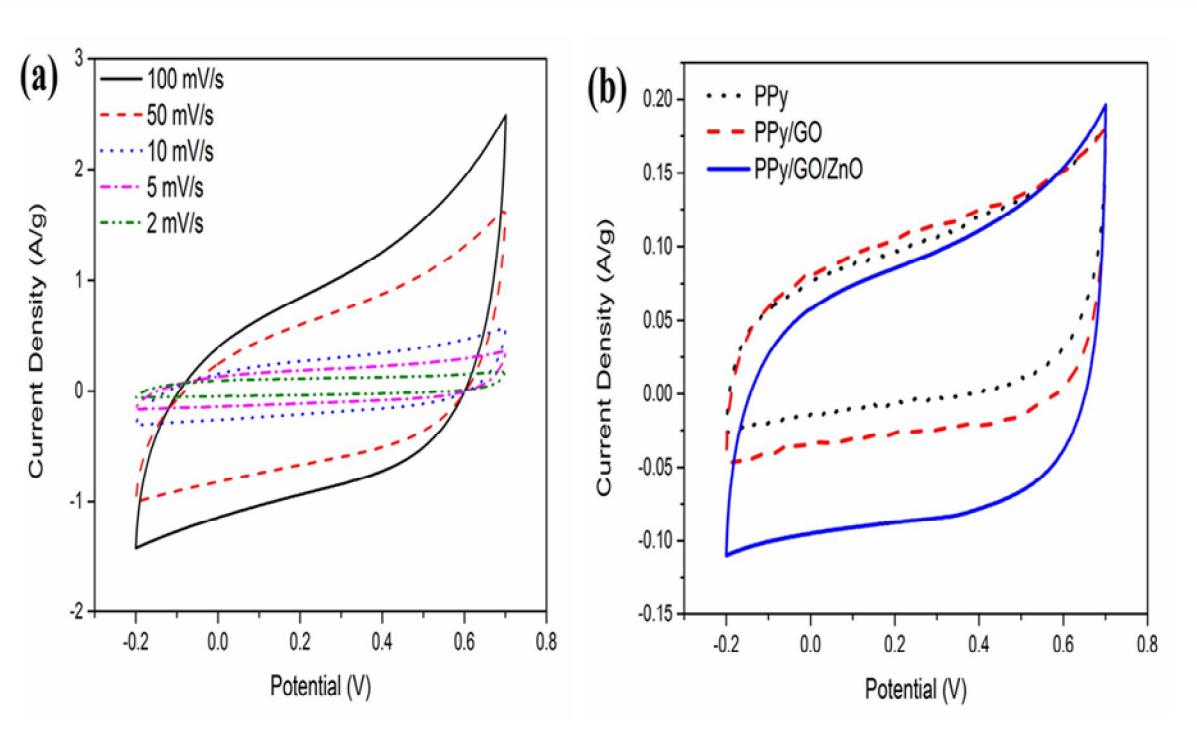

Figure 4

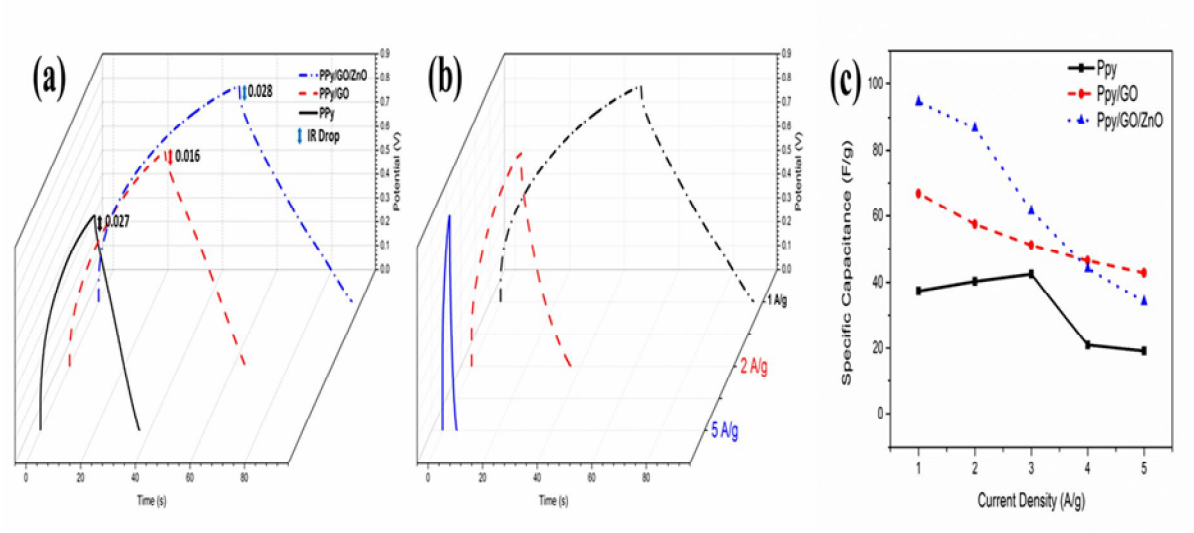

Figure 5

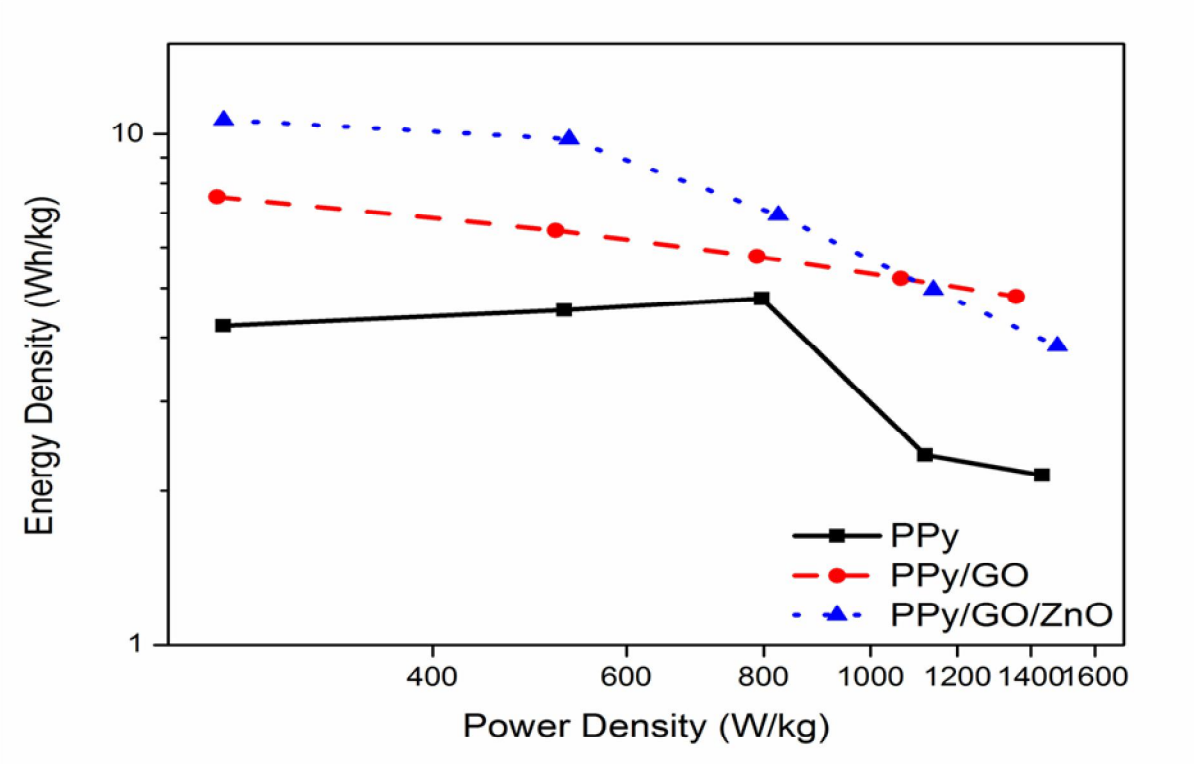

Figure 6

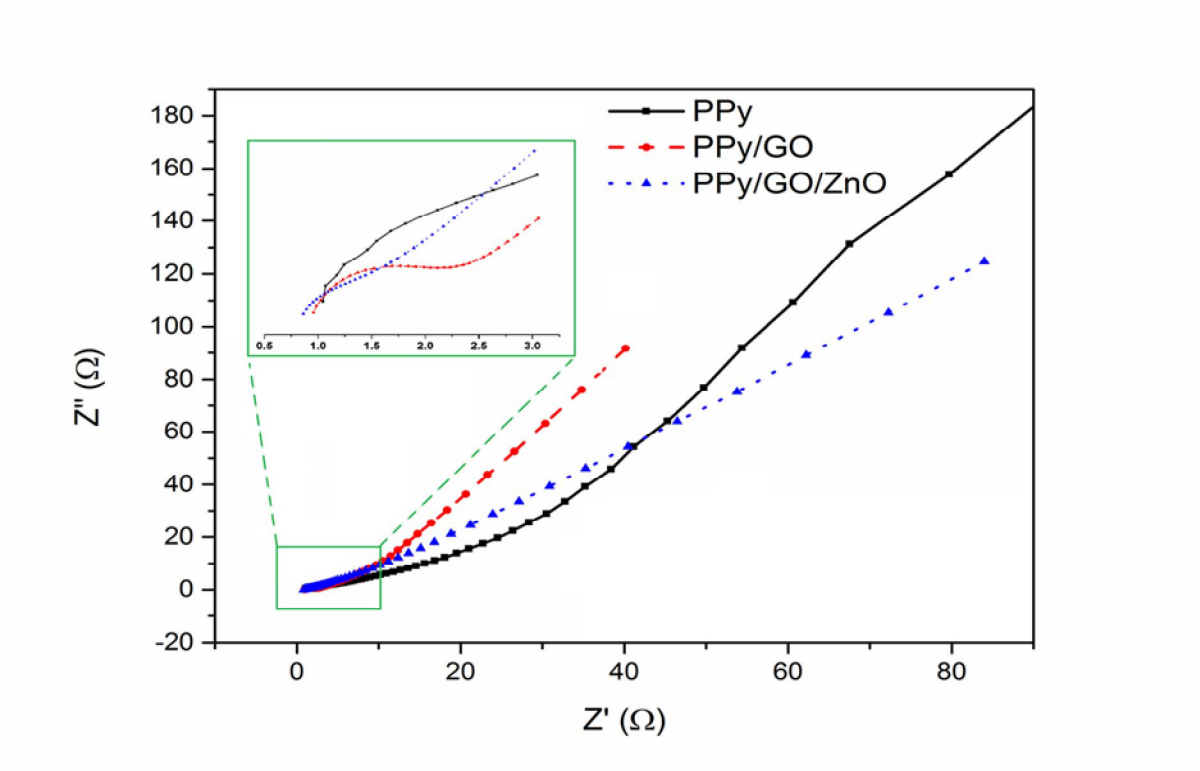

Figure 7

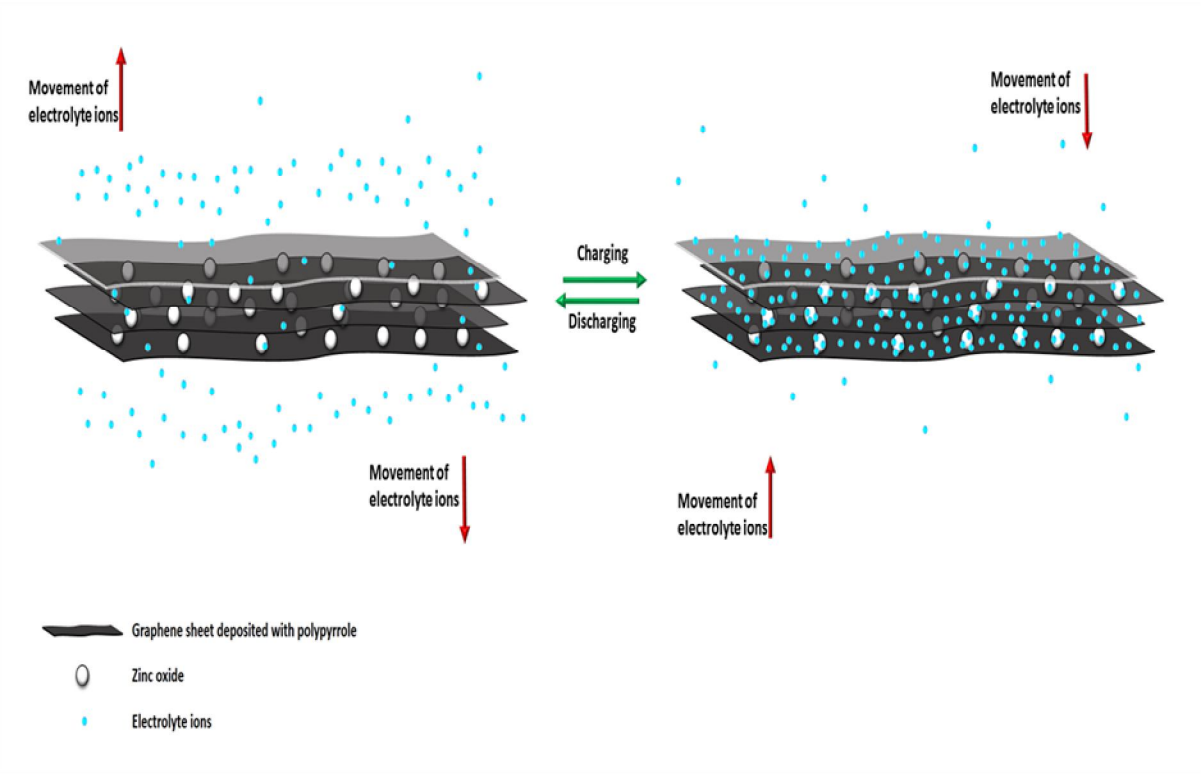

Figure 8

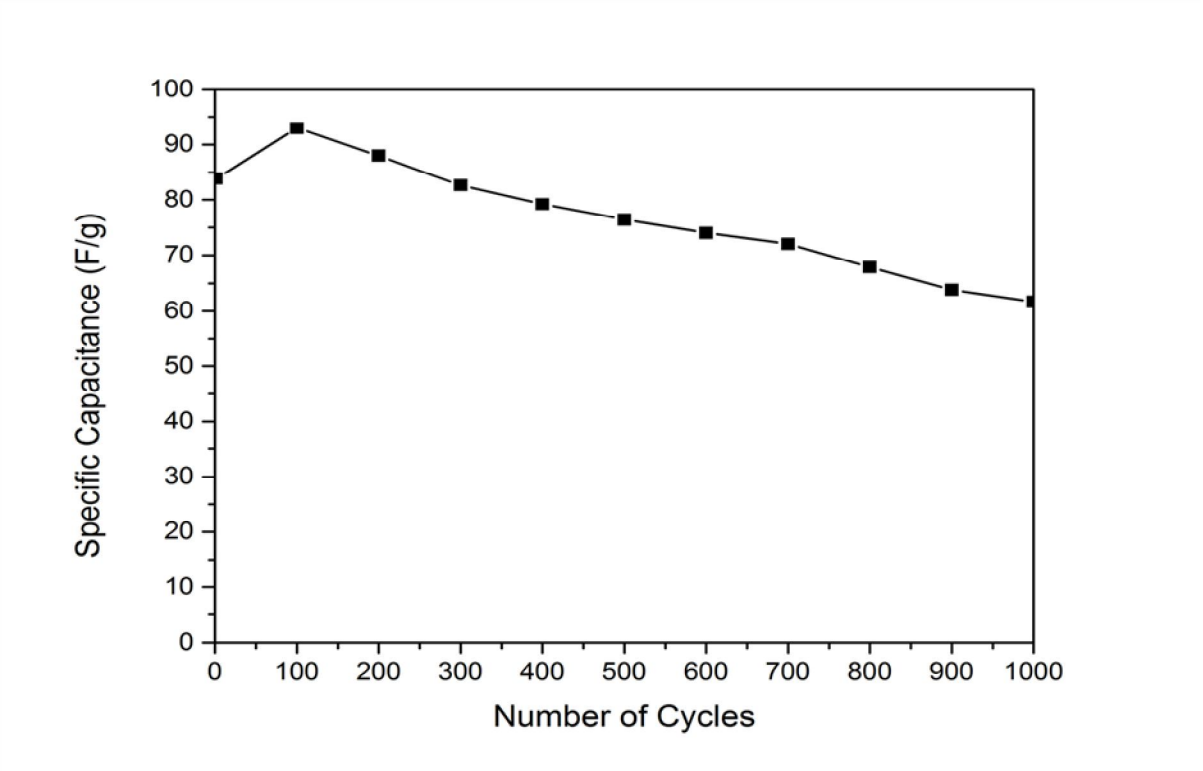

Figure 9

Table 1. Specific capacitance of PPy/GO/ZnO as a function of scan rate.

Scan rate (mV/s)	Specific Capacitance (F/g)
100	45.47
50	61.77
10	108.45
5	135.47
2	163.26